Int. J. Electrochem. Sci., 15 **(2020)** 3996 – 4004, doi: 10.20964/2020.05.07

International Journal of
ELECTROCHEMICAL
SCIENCE
www.electrochemsci.org

Hollow Mesoporous MnO_2 Spheres as Sulfur Host Materials for High-Performance Lithium-Sulfur Batteries

Yaofeng Ma

Zhengzhou Institute of Technology, Zhengzhou, 450044, China
E-mail: yfmazz1985@tom.com

Received: 9 December 2019 / *Accepted:* 6 February 2020 / *Published:* 10 April 2020

To improve the electrochemical performance of the lithium-sulfur batteries, many methods have been developed, including synthesizing advanced host materials, preparing new type electrolyte and protecting lithium anode. Among these strategies, synthesizing host materials for element sulfur is the most efficient method in improving the electrochemical performance of the lithium-sulfur batteries. In this work, we developed hollow mesoporous MnO_2 spheres as efficient host materials for the lithium-sulfur batteries. Due to the presence of the polar MnO_2, the shuttle effect of the soluble polysulfide can be greatly inhibited. As a result, the as-prepared HMOs/S composites exhibited superior cycle stability, demonstrating excellent electrochemical performance. Moreover, owing to the improved electronic conductivity, the HMOs/S composites showed much higher specific capacity than the pristine sulfur electrode.

Keywords: Li-S battery; Hollow spheres; Cycle stability; Capacity; Shuttle effect

1. INTRODUCTION

Energy consumption has become more and more rapid with the development of the technology and industry. In the past decades, energy shortage was the main issue for all the countries all over the world [1]. Therefore, it is important to promote the sustainable development of the energy in the earth [2]. As we all know, a great amount of traditional energy, such as gas [3], goal [4], have been used for the development of the science and technology [5]. However, the storage of the traditional energy is limited and non-renewable. Besides, it brings about severe air pollution for our environment. As a result, it is urgent for us to study new energy storage systems, which could replace the traditional energy [6]. During the past decades, many new energy storage systems have been developed for the applications, including supercapacitors [7], lithium-ion batteries [8], lithium-sulfur batteries [9], lithium metal batteries [10]. These energy storage systems can release high energy density and power density during the discharge and charge process via electrochemical redox reactions [11].

Among those of various energy storage systems, lithium-sulfur batteries have drawn much attraction for the researchers all over the world. This is ascribed to the high energy density (2600 Wh Kg^{-1}) and high specific capacity (1675 mAh g^{-1}) [12], which is three times than the traditional lithium-ion batteries [13]. So far, the lithium-sulfur batteries have been employed in unmanned aerial vehicle, small energy storage devices due to their advantages [14]. Meanwhile, the active materials in the lithium-sulfur batteries do not pollute the environment. As a result, many teams and personals have devoted themselves to study the lithium-sulfur batteries. However, there are still some problems which restrain the wide applications for the lithium-sulfur batteries. First, the poor electronic conductivity of the pristine sulfur leads to low active materials use during the discharging process, causing low specific capacity value [15]. Second, there is a soluble polysulfide which could form at the discharge platform of 2.3 V. These soluble polysulfides will migrate from the cathode to the anode side, which is the so-called shuttle effect [16]. Finally, the great volume change (~80%) of the sulfur causes the structural to collapse during the electrochemical reactions. Therefore, it is the key factor for researchers to solve the above three problems for improving the electrochemical performance [17].

To improve the cycle stability, many methods have been employed in the reported works. These works can be mainly concluded as the following tips: a) developing carbon-based cathode materials for the lithium-sulfur batteries, the carbon materials could improve the electronic conductivity of the whole cathode materials. b) using polar metal oxides as host materials for the lithium-sulfur batteries, which could inhibit the polysulfide migration and improve the electronic conductivity at the same time [18]. From the reported works, the employment of the metal oxides is more efficient to improve the electrochemical performance of the lithium-sulfur batteries [19].

In our work, we developed hollow mesoporous MnO_2 nanospheres as the host materials for the sublimed sulfur. The morphology of the as-prepared HMOs/S composites was observed by using scanning electron microscopy. The crystal structure was characterized by XRD. The electrochemical results indicated that the initial specific capacity of the HMOs/S composites is as high as 1501 mAh g^{-1}. In addition, the as-prepared HMOs/S composites demonstrated a superior cycling stability due to the presence of the metal oxide MnO_2. The hollow mesoporous MnO_2 spheres could provide sufficient adsorption for the soluble polysulfide. As a result, the shuttle effect of the polysulfide could be efficiently inhibited.

2. EXPERIMENTAL

2.1. Preparation of the HMOs/S composites

The hollow mesoporous MnO_2 nanospheres were prepared by hydrothermal reaction method. Typically, 1.6 g $MnSO_4$ and 3.2 g $K_2S_2O_8$ were added into 50 ml distilled water to prepare mixture solution. After that, the mixture was heated at 120 ºC for 24 h. After cooling to the room temperature, the product was collected and washed for 3 times using distilled water. As a result, the hollow mesoporous MnO_2 spheres was obtained. The HMOs/S composites were further prepared by heating the mixture of HMOs and pristine S at 155 ºC for 12 h. Finally, the HMOs/S composites can be easily

prepared.

2.2. Materials Characterization

The scanning electron microscopy (SEM) and transmission electron microscopy (TEM) were used to observe the morphology of the HMOs and HMOs/S composites. The crystal structure of the HMOs and HMOs/S composites was tested by using X-ray diffraction (XRD). The sulfur content in the HMOs/S composites was determined by thermal analysis (TG).

2.3. Materials Measurements

The electrochemical performance of the HMOs/S composites was tested by using coin half batteries. The initial discharge and charge curves were obtained by using LANDCT2001A between 1.7 and 2.6 V. Electrochemical impedance spectrum was tested on the electrochemistry workstation CHI660E at the frequency of 10 Hz~100 KHz. The adsorption test was tested by adding HMOs into the Li_2S_6 solution.

3. RESULTS AND DISCUSSION

Figure 1a shows the SEM image of the pristine MnO_2 spheres. It can be observed that the pristine MnO_2 materials exhibit nanosphere structure and demonstrate the smooth surface. Moreover, the as-prepared MnO_2 spheres are uniformly dispersed in the whole SEM image. The diameters of the MnO_2 spheres are located at 200 nm, which is beneficial for the combination with the element sulfur. Furthermore, Figure 1b displays the SEM image of the HMOs/S composites. As shown in Figure 1b, the as-prepared HMOs/S composites exhibit similar nanosphere structure.

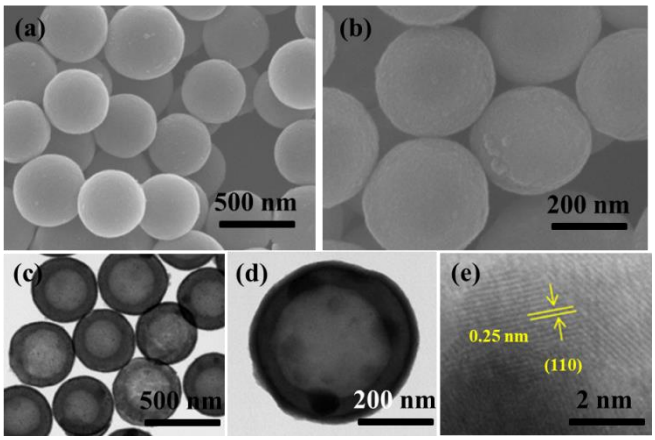

Figure 1. (a) and (b) SEM images of the pristine MnO_2 and HMOs/S composites. (c) and (d) TEM images of the HMOs/S composites. (e) HRTEM image of the HMOs/S composites.

The only difference is that the surface of the HMOs/S composites is rough. To confirm the hollow nanosphere structure, TEM images of the HMOs/S composites were displayed for the HMOs/S composites. As shown in Figure 1c and d, the hollow sphere structure can be clearly observed. With the increase of the magnification, the hollow structure can be further confirmed in Figure 1d. Besides, the sulfur layer on the surface of the hollow MnO_2 spheres is shown in Figure 1c and d. To demonstrate the presence of the MnO_2, HRTEM was conducted for the HMOs/S composites. As shown in Figure 1e, the lattice stripe for the HMOs/S composites is about 0.25 nm, which is attributed to the (110) plane of the MnO_2 [20].

Figure 2a shows the Raman spectra of the pristine MnO_2 and HMOs/S composites. It can be observed that the D and G peaks are located at 1300 cm^{-1} and 1580 cm^{-1} for the pristine MnO_2 materials, respectively [21]. Besides, the ratio of the I_D/I_G is about 1.6 for the pristine MnO_2 materials. This indicates that the as-prepared pristine MnO_2 materials have small defects [22]. However, for the as-prepared HMOs/S composites, there are great changes for the HMOs/S composites. The D and G peak are transferred from previous peaks comparing with the pristine MnO_2 materials. Moreover, the ratio of I_D/I_G is about 2.5 for the HMOs/S composites, showing much higher defects. These defects are beneficial for the employment of HMOs/S composites in the lithium-sulfur batteries. To study the porous structure, N_2 absorption and desorption isotherms were conducted for the pristine MnO_2 and HMOs/S composites. As shown in Figure 2b, the as-prepared HMOs/S composites exhibit superior mesoporous structure and high volume. This mesoporous structure could adsorb the soluble polysulfide in the lithium-sulfur battery. However, for the pristine MnO_2 materials, it shows a low volume adsorbed value compared to with the HMOs/S composites. Therefore, it can be inferred that the as-prepared HMOs materials can efficiently adsorb the soluble polysulfide. As a result, the polysulfide migration in the Li-S battery is inhibited by using the HMOs/S composites [23].

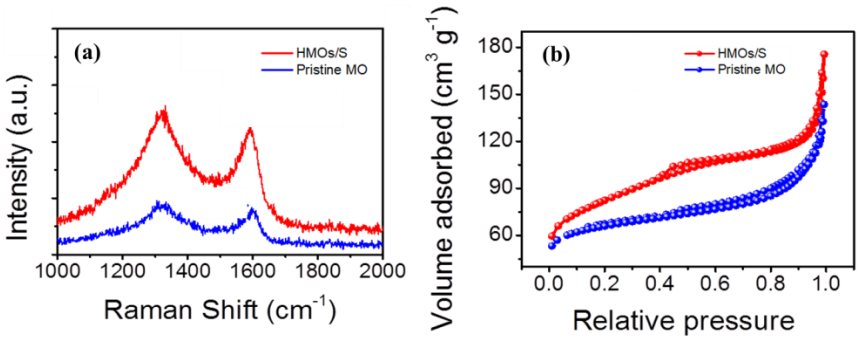

Figure 2. (a) Raman spectra of the pristine MnO_2 and HMOs/S composites. (b) N_2 absorption and desorption isotherms of the pristine MnO_2 and HMOs/S composites.

To demonstrate the crystal structure of the samples, XRD pattern was made for the HMOs and HMOs/S composites. As shown in Figure 3a, it can be observed that the pristine hollow MnO_2 spheres display typical diffraction peaks, which is the same as the reported works in the literatures. The main diffraction peaks are located at 32°, 36°, 45°, respectively. These peaks are corresponding to the crystal

planes of (110), (111) and (121), confirming the preparation of the high purity MnO_2 materials. Furthermore, after combining with the element sulfur, the as-prepared HMOs/S composites exhibit similar diffraction peaks with the pure sulfur. However, for the HMOs/S composites, the peak intensity is much weaker than the pure sulfur. This can be concluded that the HMOs/S composites were successfully synthesized. In addition, the sulfur content in the HMOs/S composites was determined by TG analysis. As shown in Figure 3b, the as-prepared HMOs/S composites have obvious weight loss between 200-260 ºC, which is ascribed to the sulfur loss. Therefore, it can be calculated that the sulfur content in the HMOs/S composites is about 78%. The obtained sulfur content for the HMOs/S composites is useful for calculating the specific capacity of the cathode materials which is used in the lithium-sulfur battery [24]. .

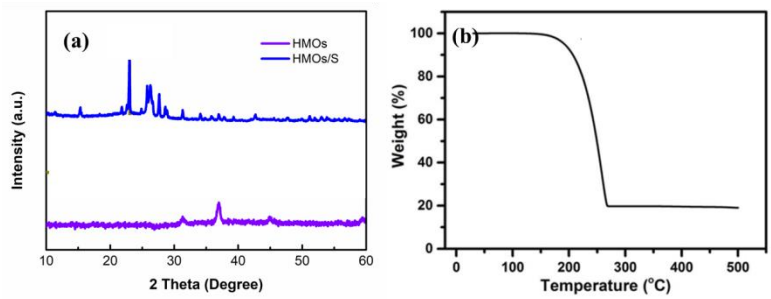

Figure 3. (a) XRD patterns of the HMOs and HMOs/S composites. (b) TG curves of the HMOs/S composites.

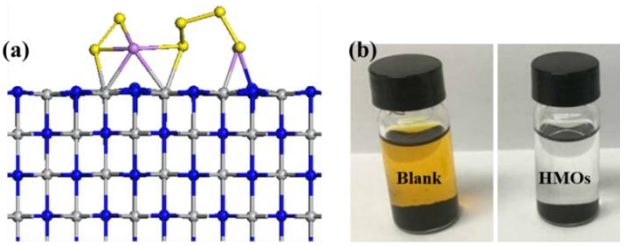

Figure 4. (a) Optimized geometries of Li_2S_6 on HMOs. (b) Adsorption test of Li_2S_6 solution by using HMOs.

To investigate the adsorption performance of the as-prepared HMOs, series of characteristics were conducted. First, optimized geometries were conducted for the HMOs. As shown in Figure 4a,, it can be clearly seen that the L_2S_6 model molecule could be steadily fixed with the HMOs structure. This result is obtained by theoretical calculation. The binding energy between HMOs and Li_2S_6 is about 0.58 eV, which could provide sufficient adsorption force for the soluble polysulfide. Furthermore, the adsorption ability was confirmed by adsorption test. As shown in Figure 4b, the pristine Li_2S_6 solution exhibits yellow color, which could be observed in the lithium-sulfur battery. After adding HMOs into the pristine Li_2S_6 solution for 20 min, it can be observed that the mixture becomes colorless, demonstrating excellent adsorption ability between the pristine Li_2S_6 and HMOs. As a result, it can be inferred that the as-prepared HMOs/S composites could exhibit superior electrochemical performance

in the lithium-sulfur battery.

Figure 5a shows the initial discharge and charge profiles of the HMOs/S composites at 0.1 C and 2 C, respectively. As shown in Figure 5a, the initial specific capacity of the HMOs/S composites is as high 1501 mAh g^{-1} at the current density of 0.1 C. When the current density was improved to 2 C, the initial specific capacity of the HMOs/S composites is about 906 mAh g^{-1} at the current density of 2 C. Besides, the other information could be obtained, that is, the DC curves of the HMOs/S composites consist of two discharge voltage platforms at 2.3 V and 2.1 V, respectively. The platform at 2.3 V is related to the transformation of sublimed sulfur to high polysulfide. The platform at 2.1 V is corresponding to the further reaction from polysulfide to Li_2S. The main specific capacity values are from this two voltage platforms. However, for the pristine S electrode, the initial specific capacity is only 1368 mAh g^{-1} at the current density of 0.1 C. The initial specific capacity of the pristine S electrode is only 601 mAh g^{-1} at the current density of 2 C, which is much lower than the HMOs/S composites. In all, the as-prepared HMOs/S composites exhibit much higher specific capacity value than the pristine S electrode. This can be attributed to the presence of the hollow MnO_2 nanofibers, which can improve the electronic conductivity of the cathode [25].

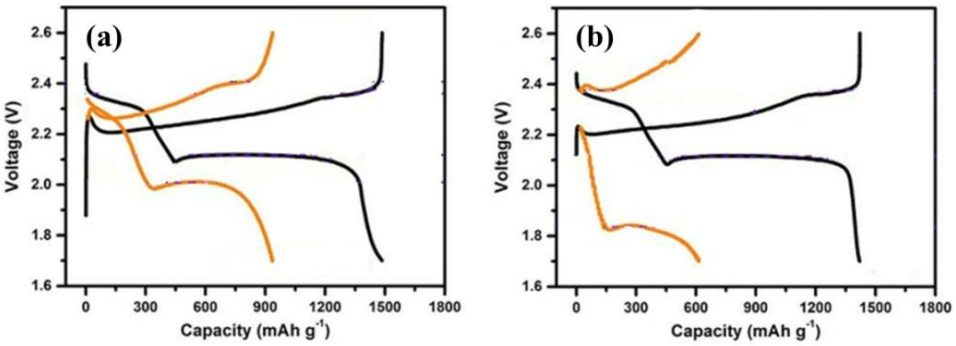

Figure 5. (a) and (b) The initial discharge and charge profiles of the HMOs/S cathode and pristine S cathode at 0.1 C and 2 C, respectively.

To further demonstrate the high electrochemical performance of the HMOs/S composites, electrochemical impedance spectrum was made for the pristine S and HMOs/S electrode. As shown in Figure 6a, the EIS of the samples consist of two parts: semicircle in the high frequency and line in the low frequency. The semicircle represents the charge transfer resistance between the electrode surface and electrolyte. The line in the low frequency is related to the Warburg impedance, which is related to the transport of the lithium-ions. Clearly, it can be concluded that the as-prepared HMOs/S composites exhibit smaller resistance than the pristine S electrode, demonstrating superior electronic conductivity. This result is consistent with the DC curves. The HMOs/S composites show much higher specific capacity value than the pristine S electrode. Figure 6b shows the cycle performance of the HMOs/S composites. The as-prepared HMOs/S composites exhibit superior cycle stability with high capacity retention of 86% after 120 cycles at the current density of 2 C. To demonstrate the efficient inhibition

for the shuttle effect, the current of shuttle effect was displayed in Figure 6c. As shown in Figure 6c, the shuttle effect current of the HMOs/S composites is nearly 0 A with the increase of the time. However, for the pristine S electrode, the shuttle effect could reach $6*10^{-5}$ A with the increasing time. Therefore, the as-prepared HMOs/S composites have long cycle stability and high specific capacity value than the pristine S electrode, which is due to the superior adsorption ability between the HMOs and soluble polysulfide in the electrolyte. Moreover, the mesoporous structure could provide sufficient space for the storage of the polysulfide. As a result, the as-prepared HMOs/S composites can be used as cathode materials for the lithium-sulfur battery. And the HMOs/S composites show high specific capacity and excellent cycle stability [26].

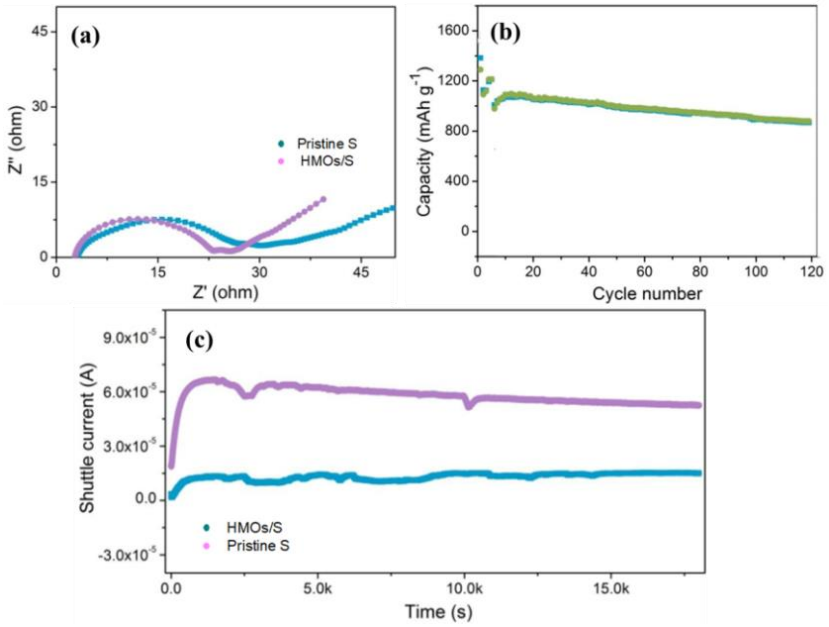

Figure 6. (a) Electrochemical impedance spectrum of the pristine S and HMOs/S cathode. (b) Cycle stability of the HMOs/S cathode at the current density of 1 C. (c) Shuttle effect current of the pristine S and HMOs/S cathode.

To further investigate the superior electrochemical performance of the HMOs/S composites, we made a new table to compare the electrochemical performance of the HMOs/S composites with other reported similar cathode materials for the lithium-sulfur batteries. As listed in Table 1, the as-prepared in this work shows high capacity retention of 86% after 120 electrochemical cycles at high current density of 2 C, which is very important for judging the electrochemical performance of the lithium-sulfur battery. Whereas, other listed cathode materials exhibit bad performance, demonstrating severe capacity fading during the electrochemical cycles. Clearly, the as-prepared HMOs/S composites can be acted as cathode materials for the lithium-sulfur batteries. Thus, the polysulfide migration is efficiently inhibited during the discharging process at the different current densities. This is mainly due to the hollow MnO_2 nanofibers, which can improve the electronic conductivity and inhibit the shuttle effect of the polysulfide at the same time.

Table 1. Comparison of the electrochemical performance of the HMOs/S cathode with other similar electrode materials.

Electrodes	Rate	Capacity	Ref
MoS_2@C	0.5 C	82% (100 cycles)	27
MoS_2/CNT	0.2 C	83% (100 cycles)	28
MoS_2/graphene	2 C	78% (100 cycles)	29
MoS_2/CNCA/S	0.2 C	81% (100 cycles)	30
HMOs/S	2 C	86% (120 cycles)	This work

4. CONCLUSIONS

In summary, hollow mesoporous MnO_2 spheres were successfully synthesized via hydrothermal reaction at 120℃. The as-prepared MnO_2 materials exhibited hollow nanosphere structure, which can act as storage device for the sublimed sulfur. After that, the HMOs/S composites were prepared by using heating method at 155 ℃ for 12 h. As a result, the HMOs/S composites were developed and designed as cathode materials for the lithium-sulfur batteries. The initial specific capacity of the HMOs/S composites was as high as 1501 mAh g^{-1} at the current density of 0.1 C. Moreover, the as-prepared HOMs/S composites displayed high capacity retention of 86% after 120 cycles at the current density of 2 C. Therefore, our work may provide a new strategy for developing cathode materials for high-performance lithium-sulfur batteries.

ACKNOWLEDGEMENT
This work is financially supported by Key Young Teachers Project of Henan Province in 2019 (2019GGJS271) and Youth Innovation Fund Project of Zhengzhou Institute of Technology (QNCXJJ2019K1).

References

1. Z. W. Seh, Y. M. Sun, Q. F. Zhang and Y. Cui, *Chem. Soc. Rev*., 45 (2016) 5605.
2. B. Li, H. F. Xu, Y. Ma and S. B. Yang, *Nanoscale Horiz*., 4 (2019) 77.
3. L. Carbone, S. G. Greenbaum and J. Hassoun, *Sustainable Energy Fuels*, 1 (2017) 228.
4. Y. Li, B. Shi, W. Liu, R. Guo, H. J. Pei, D. X. Ye, J. Y. Xie and J. L. Kong, *Electrochim. Acta*, 260 (2018) 912.
5. N. Li, Z. Weng, Y. R. Wang, F. Li, H. M. Cheng and H. S. Zhou, *Energy Environ. Sci*., 7 (2014) 3307.
6. C. Zhang, Y. Lin and J. Liu, *J. Mater. Chem. A*, 3 (2015) 10760.
7. S. Y. Bai, K. Zhu, S. C. Wu, Y. R. Wang, J. Yi, M. Ishida and H. S. Zhou, *J. Mater. Chem.* A, 4 (2016) 16812.
8. X. K. Huang, K. Y. Shi, J. Yang, G. Mao and J. H. Chen, *J. Power Sources*, 356 (2017) 72.
9. J. H. Zhou, S. J. Li, W. Sun, X. B. Ji and Y. Yang, *Inorg. Chem. Front*., 6 (2019) 1217.
10. Z. J. Liu, B. L. Liu, P. Q. Guo, X. N. Shang, M. Z. Lv, D. Q. Liu and D. Y. He, *Electrochim. Acta*,

269 (2018) 180.
11. A. Chen, W. F. Liu, H. Hu, T. Chen, B. L. Ling and K. Y. Liu, *J. Mater. Chem. A*, 6 (2018) 20083.
12. J. Q. Liu, C. Wang, J. Q. Cui, J. Li, Q. H. Li, M. Liu and Y. Xi, *RSC Adv*., 9 (2019) 12331.
13. C. B. Bucur, M. Jones, M. Kopylov, J. Spear and J. Muldoon, *Energy Environ. Sci*., 10 (2017) 905.
14. R. Steudel and T. Chivers, *Chem. Soc. Rev*., 48 (2019) 3279.
15. S. N. Yang, Y. Cheng, X. Xiao and H. Pang, *Chem. Eng. J*., 384 (2020) 123294.
16. H. B. Lin, L. Q. Yang, X. Jiang, G. C. Li, T. R. Zhang, Q. F. Yao, G. W. Zheng and J. Y. Lee, *Energy Environ. Sci*., 10 (2017) 1476.
17. K. X. Liao, S. T. Chen, H. H. Wei, J. C. Fan, Q. J. Xu and Y. L. Min, *J. Mater. Chem. A*, 6 (2018) 23062.
18. J. J. Chen, Q. Zhang, Y. N. Shi, L. L. Qin, Y. Cao, M. S. Zheng and Q. F. Dong, *Phys. Chem. Chem. Phys*., 14 (2012) 5376.
19. Q. Zhao, Q. Z. Zhu, J. W. Miao, P. Zhang and B. Xu, *Nanoscale*, 11 (2019) 8442.
20. Y. Zheng, S. S. Zheng, H. G. Xue and H. Pang, *J. Mater. Chem. A*, 7 (2019) 3469.
21. W. W. Tang, Y. Q. Zhang, W. Zhong, M. K. Aslam, B. S. Guo, S. J. Bao and M. W. Xu, *Nanoscale*, 11 (2019) 15648.
22. Y. X. Song, Y. Shi, J. Wan, S. Y. Lang, X. C. Hu, H. J. Yan, B. Liu, Y. G. Guo, R. Wen and L. J. Wan, *Energy. Environ. Sci*., 12 (2019) 2496.
23. C. S. Chai, H. Tan, X. Y. Fan and K. Huang, *J. Alloys Compd*., 820 (2020) 153144.
24. Q. Zhang, X. F. Zhang, M. Li, J. Q. Liu and Y. C. Wu, *Appl. Surf. Sci*., 487 (2019) 452.
25. H. Wei, Y. S. Ding, H. Li, Q. Zhang and Z. Yang, *Electrochim. Acta*, 327 (2019) 134994.
26. Y. You, Y. W. Ye, M. L. Wei, W. J. Sun and J. Xu, *Chem. Eng. J*., 355 (2019) 671.
27. Y. Zhong, Q. Y. Zhuang, C. M. Mao, Z. Y. Xu, Z. Y. Guo and G. C. Li, *J. Alloys Compd*., 745 (2018) 8.
28. L. J. Yan, N. N. Luo, W. B. Kong, S. Luo, H. C. Wu, K. L. Jiang, Q. Q. Li, S. S. Fan, W. H. Duan and J. P. Wang, J. Power Sources, 389 (2018) 169.
29. P. Q. Guo, D. Q. Liu, Z. J. Liu, X. N. Shang and D. Y. He, *Electrochim. Acta*, 256 (2017) 28.
30. X. L. Li, K. Zhao, L. Y. Zhang, Z. Q. Ding and K. Hu, *J. Alloys Compd*., 692 (2017) 40.